Universiteit Antwerpen

This item is the archived peer-reviewed author-version of:

VEGF-targeted magnetic nanoparticles for MRI visualization of brain tumor

Reference:

Abakumov MaximA., Nukolova Natalia V., Sokolsky-Papkov Marina, Abakumov Artem M., et al..- VEGF-targeted magnetic nanoparticles for MRI visualization of brain tumor

Nanomedicine: nanotechnology, biology and medicine - ISSN 1549-9634 - 11:4(2015), p. 825-833

Full text (Publishers DOI): http://dx.doi.org/doi:10.1016/j.nano.2014.12.011

To cite this reference: http://hdl.handle.net/10067/1263510151162165141

uantwerpen.be

Institutional repository IRUA

Accepted Manuscript

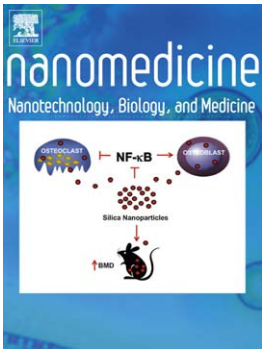

VEGF-targeted magnetic nanoparticles for MRI visualization of brain tumor

M.A. Abakumov Ph.D., N.V. Nukolova Ph.D., M. Sokolsky-Papkov Ph.D., S.A. Shein Ph.D., T.O. Sandalova M.Sc, H. Vishwasrao M.Sc, N.F. Grinenko Ph.D., I.L. Gubsky M.Sc, A.M. Abakumov Ph.D., A.V. Kabanov Ph.D., Dr.Sci., V.P. Chekhonin Ph.D., Dr.Sci.

PII: S1549-9634(15)00017-9
DOI: doi: 10.1016/j.nano.2014.12.011
Reference: NANO 1045

To appear in: *Nanomedicine: Nanotechnology, Biology, and Medicine*

Received date: 19 February 2014
Revised date: 2 December 2014
Accepted date: 13 December 2014

Please cite this article as: Abakumov MA, Nukolova NV, Sokolsky-Papkov M, Shein SA, Sandalova TO, Vishwasrao H, Grinenko NF, Gubsky IL, Abakumov AM, Kabanov AV, Chekhonin VP, VEGF-targeted magnetic nanoparticles for MRI visualization of brain tumor, *Nanomedicine: Nanotechnology, Biology, and Medicine* (2015), doi: 10.1016/j.nano.2014.12.011

This is a PDF file of an unedited manuscript that has been accepted for publication. As a service to our customers we are providing this early version of the manuscript. The manuscript will undergo copyediting, typesetting, and review of the resulting proof before it is published in its final form. Please note that during the production process errors may be discovered which could affect the content, and all legal disclaimers that apply to the journal pertain.

ACCEPTED MANUSCRIPT

VEGF-targeted magnetic nanoparticles for MRI visualization of brain tumor

M.A. Abakumov,[†,#] N.V. Nukolova,[†,*,#] M. Sokolsky-Papkov,[§] S.A. Shein,[*] T.O. Sandalova,[*] H. Vishwasrao,[§,¶] N.F. Grinenko,[*] I.L. Gubsky,[†] A.M. Abakumov,[∫] A.V. Kabanov,[§,#] and V.P. Chekhonin[†,*]

[†] Department of Medical Nanobiotechnology, Pirogov Russian National Research Medical University, Moscow, Russia

[*] Division of Fundamental and Applied Neurobiology, Serbsky State Research Center of Social and Forensic Psychiatry, Moscow, Russia

[#] Laboratory of Chemical Design of Bionanomaterials, Chemistry Department, M.V. Lomonosov Moscow State University, Moscow, Russia

[¶] Center for Drug Delivery and Nanomedicine, Department of Pharmaceutical Sciences, College of Pharmacy, University of Nebraska Medical Center, Omaha, Nebraska, USA.

[§] Center for Nanotechnology in Drug Delivery and Division of Molecular Therapeutics, UNC Eshelman School of Pharmacy, University of North Carolina at Chapel Hill, Chapel Hill, NC 27599-7362, USA

[∫] Electron Microscopy for Materials Science (EMAT), University of Antwerp, Groenenborgerlaan 171, Belgium

Corresponding author:

Name: Maxim A. Abakumov

Address: Russia, Moscow, Ostrovityanova st,1

Tel: +7903586477

Email: abakumov1988@gmail.com

Abstract word count: 137

Complete manuscript word count: 4996

Number of references: 26

Number of figures: 6

Number of tables: 1

ACCEPTED MANUSCRIPT

Authors academic degrees:

M.A. Abakumov - Ph.D.

N.V. Nukolova - Ph.D.

M. Sokolsky-Papkov - Ph.D.

S.A. Shein - Ph.D.

T.O. Sandalova - M.Sc

H. Vishwasrao – M.Sc

N.F. Grinenko - Ph.D.

I.L. Gubsky – M.Sc

A.M. Abakumov - Ph.D.

A.V. Kabanov - Ph.D., Dr.Sci.

V.P. Chekhonin - Ph.D., Dr.Sci.

This work was supported by grant of Russian Federation Ministry of Science and Education grant (11.G34.31.0004), grants of RSF 14-15-00698 (PK study and cytotoxicity) and 14-13-00731 (MRI imaging), grant of RFBR 13-04-01383A.
No competing interests are present in this paper.

ACCEPTED MANUSCRIPT

ACCEPTED MANUSCRIPT

ABSTRACT

This work is focused on synthesis and characterization of targeted magnetic nanoparticles as magnetic resonance imaging (MRI) agents for *in vivo* visualization of gliomas. Ferric oxide (Fe_3O_4) cores were synthesized by thermal decomposition and coated with bovine serum albumin (BSA) to form nanoparticles with D_{eff} of 53±9 nm. The BSA was further cross-linked to improve colloidal stability. Monoclonal antibodies against vascular endothelial growth factor (mAbVEGF) were covalently conjugated to BSA through a polyethyleneglycol linker. Here we demonstrate that 1) BSA coated nanoparticles are stable and non-toxic to different cells at concentration up to 2.5 mg/mL; 2) conjugation of monoclonal antibodies to nanoparticles promotes their binding to VEGF-positive glioma C6 cells *in vitro*; 3) targeted nanoparticles are effective in MRI visualization of the intracranial glioma. Thus, mAbVEGF-targeted BSA-coated magnetic nanoparticles are promising MRI contrast agents for glioma visualization.

ACCEPTED MANUSCRIPT

ACCEPTED MANUSCRIPT

BACKGROUND

Gliomas make up 80% of all malignant brain tumors and are characterized by fast progression and invasive character. Due to current diagnostic limitations, surgery is performed in advanced stage of the disease when the tumor has already infiltrated deeply into the surrounding tissues. At this stage it is impossible to remove the tumor with all the invasion cords without irreversible disruption of the patient brain function. Moreover, high-grade gliomas are highly resistant to chemical and radiation therapy, which leads to about 100% relapse rate and median survival of 12-14 months after diagnosis.[1]

Magnetic resonance imaging (MRI) is one of the leading methods for diagnosis of brain malignancies.[2] MRI contrast agents are divided into T1 and T2 categories according to their ability to interact with magnetic field. T1 contrast agents are mainly transition metal ion complexes with different chelating agents, in particular Gd(III). However, most of commercially available Gd(III) chelates have short half-life in the body and are excreted 20 min after intravenous (*i.v.*) injection. [3] The exception can be made for Ablavar®, being Gd chelate which reversibly bind to blood albumin and provide 1 hour window for imaging. [4] T2 contrast agents include magnetic nanoparticles (MNPs), mainly γ-Fe_2O_3 and Fe_3O_4. These iron oxides nanoparticles are superparamagnetic when the diameter of the magnetic nuclei is below 20 nm and have high magnetization. [5,6] Bare MNPs are non-toxic, however, they aggregate in water and require surface modifications to form stable colloidal dispersions. High molecular weight compounds such as dextran[7], chitosan[8], polyethylene glycol[9] have being used as coating agents. Furthermore, surface modifications may strongly affect the aggregation behavior and the particle size of MNPs, which alter the blood circulation time,[10] as well as T2 relaxivity values.[11] Current procedures of surface modification rely either on ligand exchange process or on ionic and electrostatic interactions between the bare nanoparticles surface and coating agent, which strongly depend on the pH and ionic strength of the solution. Desorption of the coating agent during blood circulation or its exchange with the plasma compounds can result in

ACCEPTED MANUSCRIPT

nanoparticles aggregation, non-specific uptake by cells of the mononuclear phagocyte system and enhanced clearance. [12] Moreover, for targeted MNPs, desorption of the coating may result in decrease in targeting efficiency due to the loss of targeting moieties. [13] To overcome these shortcomings a stabilization of the coatings of MNP by cross-linking may be useful. Such stabilized coating can be further decorated with tumor specific targeting moieties to enhance delivery of MNPs to tumors.

It is known that high-grade gliomas have extensive areas of necrosis and hypoxia, which up-regulates angiogenesis including secretion of pro-angiogenic factors, mainly vascular endothelial growth factor (VEGF).[14] Enhanced accumulation of VEGF in extracellular matrix and cell membranes stimulates growth of blood vessels within the tumor. [15,16] Furthermore, progression of the brain tumors is associated with increased leakiness and permeability of the blood–brain barrier (BBB), which can facilitate penetration of macromolecules and nanoparticles (up to 150 — 200 nm) directly into interstitial space. [17]Taken together, this may result in successful brain penetration and retention of nanoparticles, modified with antibodies against tumor-specific or endothelium-specific antigens.

In this study we report enhanced visualization of intracranial glioma using iron oxide nanoparticles modified with monoclonal (mAb) anti VEGF antibodies (mAbVEGF). The results suggest that 1) cross-linking of coating layer (in our case bovine serum albumin, BSA) can improve stability and biocompatibility of the MNPs; 2) conjugation of anti-VEGF antibodies to the nanoparticle surface increases the accumulation of the nanoparticles in glioma C6 cells therefore allows selective visualization of the intracranial glioma in a rat model.

ACCEPTED MANUSCRIPT

MATERIALS AND METHODS

Iron (III) acetylacetonate, benzyl alcohol, glutaric dyaldehyde, *N*-(3-dimethylamino-propyl)-*N′*-ethylcarbodiimidehydrochloride (EDC), N-hydroxysuccinimide (NHS) and other chemicals and solvents were purchased from Sigma-Aldrich (USA). Amino-polyethyleneglycol-7500-maleimide (NH_2-PEG-MAL) was from CreativePEGWorks, USA. Alexa Fluor 488 labeled Goat anti-mouse IgG antibodies were purchased from Invitrogen, USA. Monoclonal anti VEGF antibodies and non-specific murine immunoglobulin G (IgG) were obtained as previously described .[18]

Rat glioma C6, rat astrocytes, and HEK293 cells were cultured in the DMEM medium (Life Technologies, Grand Island, NY) containing 2 mM glutamine and supplemented with 10% (v/v) FBS, 100 U/mL penicillin and 0.1 mg/mL streptomycin at 37°C in a humidified atmosphere containing 5% CO_2. Cells were harvested at 80% confluence using trypsin-EDTA (Life Technologies, Grand Island, NY).

Synthesis of MNPs coated with BSA (MNP-BSA)

The solution of iron(III) acetylacetonate (2 g) in anhydrous benzyl alcohol (40 mL) was heated to 110°C for 1h. After 1h the solution was heated to reflux temperature and kept under reflux for 40h under nitrogen atmosphere. After 40h, the solution was cooled down and MNPs were precipitated by acetone, thoroughly washed with acetone, and dried. The aqueous dispersion of MNPs was coated with bovine serum albumin (BSA). 20 mg of the dried nanoparticles were dispersed in 5 mL of distilled water, pH of the dispersion was adjusted to 11.0 using 1M NaOH and clear solution was observed. The clear solution was sonicated for 10 min. 40 mg of BSA in 5 mL of water, pH 11.0 was added to the MNPs solution. The mixture was incubated at room temperature (r.t.) for 4h with constant stirring and dialyzed against distilled water (MWCO 12 kDa, Sigma-Aldrich, USA) for 2 days (water was replaced 4 times). After dialysis, MNP-BSA nanoparticles solution was stored at 4˚C.

ACCEPTED MANUSCRIPT

Synthesis of cross-linked MNP-BSA nanoparticles (MNP-BSA_{Cl})

500 µl of 1M NaOH were added to 20 ml of aqueous solution of MNP-BSA (2 mg/mL Fe_3O_4, 4 mg/mL BSA). After pH adjustment, 2.3 mL of 25% water solution of glutaric aldehyde were added drop-wise with constant stirring. The mixture stirred for 15min and the excess of glutaric aldehyde was inactivated by 500 µl of 3 M glycine, pH 9.2. After that 1 mL of sodium borohydride solution (4 mg/mL) was added and the mixture was stirred for 60min at r.t. The nanoparticles were purified from the by-products by filter centrifugation using Amicon centrifuge filters (MWCO 100 kDa, Amicon). MNP-BSA_{Cl} were purified from cross-linked and non-cross-linked BSA by gel-filtration chromatography (Sepharose CL-6B, separation range 10 - 4000 kDa, column 70 × 2.5 cm, flow speed 0.5 mL/min, PBS).

Conjugation MNP-BSA_{Cl} with mAbVEGF

0.5 mL of mAbVEGF solution (500 µg/mL) in 0.1 M carbonate buffer, pH 8.6 were incubated with 16 µL of 14 mM solution of Traut's reagent for 1h at r.t. The excess of the Traut's reagent was removed by gel-filtration on Sephadex G-25. 20 µL of NH_2-PEG-MAL (40 mg/mL) in dimethylsulfoxide were added to the solution of thiolated antibodies and the mixture was incubated for 4h at 4°C. To activate the carboxylic groups of MNP-BSA_{Cl}, 1 mL of MNP-BSA_{Cl} solution (4.5 mg/mL) in distilled water and 8 µL of EDC solution (8 mg/mL in distilled water) and 10 µL of NHS solution (40 mg/mL) in distilled water. The solution of PEGylated antibodies was added to activated nanoparticles solution and the mixture was incubated for 2h at 4°C. Ligand modified nanoparticles (MNP-BSA_{Cl}-mAbVEGF) was purified from unbound antibodies by gel-filtration on Sepharose CL-6B (PBS, column 50 × 2.5 cm, 0.5 mL/min). Similar procedure was used for synthesis and purification of the IgG modified nanoparticles.

ACCEPTED MANUSCRIPT

Biodistribution of MNP-BSA$_{Cl}$

Tyrosine residues in BSA on the nanoparticles surface were labeled with ^{125}I using chloramine method. [19] First, 40 µL of $Na^{125}I$ solution with specific activity of 1 GBq were added to 1.2 mL of MNP-BSA solution in PBS (25 mg/mL). Second, 100 µL of chloramine solution (10 mg/mL) were added and the solution was incubated for 5min. Reaction was terminated by addition of 100 µL of sodium thiosulfate (10 mg/ml). Excess of non-reacted iodine was removed by gel-filtration on Sepadex-G25. Labeling efficiency was 30%.

10-week old Wistar rats (n = 4) were injected *i.v.* with 3×10^8 Bq/kg of radioactively labeled NMP-BSA. Blood samples were collected 1, 10 min and 1, 8,16, 24 h after injection into heparin containing tubes. After 24h animals were injected with 200 mg/kg ketamine and perfused with 400 mL of 0.9 % NaCl in accordance with a previously reported procedure.[20] After perfusion the animals were decapitated and the brain and organs were collected. The specific radioactivity for each organ was determined using gamma counter (Rack Beta II). To determine the radioactivity readings of the desorbed BSA, blood cells were isolated by centrifugation (3000g, 30 min) and the protein fraction was precipitated with 50 % trichloroacetic acid.

MRI visualization of glioma C6 *in vivo*

MRI studies were performed on rats bearing experimental glioma C6 (3 groups, n = 4). Animals (10-week old Wistar rats, an average weight of 260 g) were anesthetized by intraperitoneal injection of ketamine (50 mg/kg) and diazepam (5 mg/kg). Experimental glioma was established by intracerebral stereotactic implantation of C6 glioma cells (4×10^5 cells per animal). Cells were implanted into striatum region at coordinates Ap -1.0; L 3.0; V 4.5, TBS -5 mm according to the Swanson's rat brain atlas[21] using stereotaxic system (Narishige, Japan) and Quintessential Stereotaxic Injector (Stoelting, USA). After 2 weeks, the glioma was confirmed by T2 weighted MRI, animals were *i.v.* injected with solution of MNP-BSA$_{Cl}$-mAbVEGF/ MNP-BSA$_{Cl}$-IgG or Feridex (12 mg/kg Fe, 16 mg/kg Fe_3O_4). Animals were scanned before the

ACCEPTED MANUSCRIPT

injection, 5 min and 24 h after injection on the MRI tomograph Clinscan 7T (Bruker, USA) in SWI regime. TurboSpinEcho scan parameters were following: TR = 4500 ms, TE = 49 ms, echo train length = 7, base resolution 320x320, FOV 40x40 mm, flip angle = 180°, slice thickness= 0.5 mm. SWI scan parameters were following: TR = 40 ms, and TE = 29 ms, base resolution 320x230, FOV 45x32 mm, flip angle 15°, slice thickness 0.5 mm.

RESULTS

MNPs were synthesized by thermal decomposition of iron(III) acetylacetonate. The diameters of the iron oxide cores of these nanoparticles were in the 5-10 nm range as measured by TEM (Figure 1A). The ring electron diffraction analysis confirmed that the obtained MNPs were nanocrystals with a face-centered cubic lattice characteristic of magnetite, Fe_3O_4 with the unit cell parameter $a \approx 0.84$ nm (Figure 1B).

To stabilize MNPs in the aqueous dispersion at physiological pH the MNPs were coated with BSA. The obtained BSA-coated MNPs (MNP-BSA) were relatively uniform (PDI 0.19) as determined by DLS, and their effective diameters and ζ-potential in distilled water were 53 ± 9 nm and -41 ± 6 mV, respectively (Table 1). HAADF-STEM studies suggested that similarly to uncoated MNPs the MNP-BSA had a spherical morphology (Figure 2A, Figure 1A). Since the signal on the HAADF-STEM images is proportional to average atomic number, the particles look prominently bright, demonstrating high crystallinity and being surrounded by amorphous BSA shell. The separate nanoparticles with individual covering containing carbon and oxygen atoms (Figure 2B, bottom panel), which refer to different fragments of protein BSA detected by compositional analysis using EDX.

Desorption of the protein molecules from the surface of MNPs either 1) during their shelf storage or 2) upon their exposure to plasma in the body may result in the loss of the stability of the protein-coated MNPs.[12] We observed aggregation of MNP-BSA after their centrifugation using Amicon filters (MWCO 100 kDa, 2,000 rpm, 3 cycles, water, 4°C). The centrifuge

ACCEPTED MANUSCRIPT

filtration resulted in separation of 43% of the initial BSA in the formulation, which was detected in the filtrate. Evidently, the removal of the BSA from the surrounding media could shift equilibrium and facilitate BSA desorption from the MNP-BSA. Along with the increased concentration of nanoparticles after centrifuge filtration, this can promote the nanoparticles aggregation.

Therefore, in an attempt to form stable BSA coating and prevent aggregation of MNPs we cross-linked the absorbed BSA molecules by glutaric aldehyde. After cross-linking the particle size of MNP-BSA_{Cl} increased compared to that of MNP-BSA by nearly 70% (Table 1) probably due to cross-linking of individual particles and formation of larger clusters. However, the particle effective diameters were still less than 100 nm, which we considered essential for their further *in vivo* evaluations. Analysis of MNP-BSA_{Cl} by HAADF-STEM method (Figure 2B, bottom panel) suggests that the iron oxide particles were embedded in the mount of "carbon and oxygen species", which was consistent with formation of protein cage around the MNPs.

As expected the stability of MNP-BSA_{Cl} was increased after cross-linking. The MNP-BSA_{Cl} did not lose BSA and did not aggregate after the centrifuge filtration. In the presence of added 10% fetal bovine serum (FBS) both the MNP-BSA and MNP-BSA_{Cl} displayed increase of the particle sizes followed by their gradual decrease over 10 days (Figure 3). However, for MNP-BSA_{Cl} the particle size change from day 0 to day 10 was only 15% while for MNP-BSA it was nearly 400%. Moreover, during the same time the PDI indexes for MNP-BSA were increased by over 100%, while for MNP-BSA_{Cl} the PDI changes were only about 50%. Overall, this suggests that cross-linked nanoparticles are somewhat more stable in the presence of the added serum than the non-cross-linked nanoparticles. However, one must recognize that the behavior and the underlying processes in the presence of added FBS are complex, and may include absorption of the added serum molecules at the MNPs surface, displacement of the BSA molecules by the added serum molecules (for non-cross-linked MNP-BSA) and others. Important for studies described below, the MNP-BSA_{Cl} particles could be stored in aqueous dispersion (water and

ACCEPTED MANUSCRIPT

PBS) almost without changes of the particle size (90±2 nm vs. 97±3 nm before and after storage for 3 weeks at 4°C, respectively).

The T2 relaxivity of the MNP-BSA_{Cl}, determined as a slope of the dependence of T2 relaxation time on the concentration of MNPs, was equal to 216 ± 7 $mM^{-1}s^{-1}$ (Table 1). This T2 relaxivity value was somewhat less than the T2 relaxivity of the MNP-BSA before cross-linking (260 ± 40 $mM^{-1}s^{-1}$) but still comparable to the T2 relaxivity of the Food and Drug Administration (FDA) approved MRI agent Feridex (160 ± 10 $mM^{-1}s^{-1}$). Collectively, our data suggest that BSA coating of MNPs resulted in stable nanoparticles with high T2 relaxivity values.

The cytotoxicity of obtained MNP-BSA_{Cl} was examined by MTT assay using HEK293, rat glioma C6 and rat normal astrocyte cells. In all cells the MNP-BSA_{Cl} nanoparticles were not toxic up to 2.5 mg/mL of the iron oxide (Figure 4C). This *in vitro* study served as a preliminary test of the nanoparticle safety and provided reassurance that they could be used in further *in vivo* experiments. [22]

To study the plasma half-life and biodistribution of MNP-BSA_{Cl} nanoparticles these nanoparticles were labeled by I^{125} and injected to the healthy rats. The plasma PK of MNP-BSA_{Cl} revealed two phases: the "fast" one with the plasma half-life of about 10 min and the "slow" one with the half-life of about 1h (Figure 4A). The twenty-four hours post-injection 3 ± 1 % of the injected dose remained in the blood. Analysis of the distributed radioactive label in the organs after 24h revealed that about 5 % of injected dose accumulated in the liver about 1 % in kidneys and much smaller amounts amount (< 0.1 %) in the heart, spleen, lung and brain (Figure 4B). There was a considerable accumulation of I^{125} in the thyroid gland, which suggested that the probe was cleaved off the labeled MNP-BSA_{Cl} nanoparticles.

The final step of the synthesis was the attachment of the targeting moieties to MNP-BSA_{Cl} to promote delivery of MNP to tumor cells. The mAbVEGF and IgG as a negative control were attached to the MNP-BSA_{Cl} nanoparticles through a polyethyleneglycol (PEG) linker (Fig1, Supplementary Data). First, amino groups of antibodies were converted to sulfhydryl groups by

ACCEPTED MANUSCRIPT

2-iminothiolane (Traut's reagent) and reacted with maleimide group of heterofunctional NH_2-PEG-MAL. Second, the PEGylated mAb was conjugated to NHS/EDC-activated carboxylic groups of BSA in MNP-BSA_{Cl}. Finally, unconjugated mAb was removed by gel-filtration chromatography. The resulting modified nanoparticles were concentrated on Amicon filters (MWCO 100 kDa) and stored at 4°C. These nanoparticles were negatively charged as was evident from their ζ-potential values that were practically the same as that of the initial MNP-BSA_{Cl} nanoparticles (Table 1). Interestingly, the particle size after conjugation of the mAb and IgG was somewhat decreased compared to the size of the MNP-BSA_{Cl} nanoparticles and the polydispersity was relatively low, which may be explained by the additional step of nanoparticle purification by chromatography. The T2 relaxivities of both MNP-BSA_{Cl}-mAbVEGF and MNP-BSA_{Cl}-IgG nanoparticles were around 170 $mM^{-1}s^{-1}$, which was somewhat less than that of non-targeted MNP-BSA_{Cl} but still comparable with Feridex (Table 1).

We further used ELISA assay to examine ability of targeted nanoparticles to bind with VEGF. As seen in Figure 5**C** in the ELISA experiment the MNP-BSA_{Cl}-mAbVEGF nanoparticles displayed greater binding to the substrate compared to MNP-BSA_{Cl}-IgG nanoparticles. The latter also exhibited some binding presumably due to non-specific interactions with the substrate. Next we examined the *in vitro* targeting of the nanoparticles to their receptor using the C6 glioma cells, which express membrane bound VEGF. [23,27] The immunofluorescence analysis suggested that MNP-BSA_{Cl}-mAbVEGF nanoparticles were binding with the glioma C6 cells (Figure 5A) while the MNP-BSA_{Cl}-IgG nanoparticles did not (Figure 5B). Confocal colocolization analysis of FITC-labeled MNP interaction with cells shown that after addition to C6 cells MNP were internalized by cells and mostly were transported into lysosomes (Supplementary Materials Figure 6C).

Finally, we attempted the MRI visualization of the intracranial glioma in rats using MNP-BSA_{Cl}-mAbVEGF, MNP-BSA_{Cl}-IgG and Feridex. All three MRI contrast agents were administered *i.v.* at the equivalent doses of iron oxide. The tumor area and especially tumor

ACCEPTED MANUSCRIPT

vessels were immediately seen on MRI scans after *i.v.* injection of MNP-BSA_{Cl}-IgG (Figure 6B). According to our PK data (Figure 4A), the plasma concentration of these nanoparticles rapidly decreased. Consistent with this observation 2h after nanoparticles administration the MRI picture contrast deteriorated. After 24h post-injection the signal intensity of MNP-BSA_{Cl}-IgG became very low so the images of the treated and non-treated animals were indistinguishable (compare Figure 6A and Figure 6C). In the case of VEGF-targeted MNP-BSA_{Cl}-mAbVEGF, 5 min and 2h after administration the signal intensity in the tumor tissue was similar to that of MNP-BSA_{Cl}-IgG (Figure 6E and Supplementary Materials Figure 3). However, 24h after administration the MRI contrast of the glioma was significantly higher than that of control group (Figure 6F), which can be due to the specific accumulation of MNP-BSA_{Cl}-mAbVEGF in tumor tissue. In contrast, Feridex did not show visualization of glioma under these conditions, probably owing to rapid elimination of these contrast agents (Figure 6G,H,I). [24]

DISCUSSION

MNPs are perspective contrast agents for MRI visualization of glioma. However, their magnetic properties strongly depend on the size and crystal structure.[5] The MNP synthesized in this work had highly ordered crystal structure that corresponds to spinel structure of Fe_3O_4 (Figure 1B). To prevent aggregation of MNP in the biological milieu they were stabilized by the surface-coating with BSA. The choice of BSA was rationalized by its biocompatibility and low toxicity.[25] Nanoparticles covered with BSA were stable in water and PBS for several days, although they were inclined to precipitate after removal of the adsorbed BSA by centrifuge filtration. Since equilibrium between the free and adsorbed BSA in solution was established, the removal of free BSA during filtration shifted the equilibrium, promoted desorption of adsorbed BSA and hence apparently reduced the thickness the protein layer around MNP. All these factors affected the colloidal stability of BSA-coated MNP. For stabilization of BSA on the surface of MNP, protein molecules were chemically cross-linked. Increase in the particle size after cross-

ACCEPTED MANUSCRIPT

linking was observed by DLS (Table 1). HAADF-STEM images (Figure 2) detected that cross-linked MNP-BSA nanoparticles consisted of iron oxide nanocrystalls trapped into protein cages. These nanoparticles did not release BSA and were stable upon centrifugal filtration. It appears that the introduction of covalent bonds between multiple MNP-BSA species resulted in formation of larger MNP-BSA_{Cl} nanoparticles.

It is well known that the T2 relaxivity values of MNP-based aggregates and their plasma half-life strongly depend on the size of the nanoparticles as well as the type of polymer or ligand used for surface modification of MNP. Thus, as the MNP increases the T2 relaxivity increases and plasma half-life decreases.[10,11] We labeled MNP-BSA_{Cl} by ^{125}I thought tyrosine residues of BSA to evaluate the blood circulation time and organ distribution of nanoparticles. The plasma PK of MNP-BSA_{Cl} exhibited a fast (half-life about 10min) and slow (half-life about 1h) phases, which is typical for many nanoparticles.[24] In our case this could be due to heterogeneity of MNP particle size and/or degradation of BSA-covering. Heterogeneity of MNP (polydispersity 0.196) may lead to situation when the bigger MNP with large number of ^{125}I labels are eliminated faster by filtration through the spleen and liver (fast component). Meanwhile, the smaller MNP may circulate longer in the blood generating slow component. Earlier similar two-phase curve of half-life in blood was observed for commercial contrast agent Feridex, which consists of MNP coated with dextran (hydrodynamic size 120-180 nm).[24] It is interesting to note that at 24h after injection of MNP-BSA_{Cl} the highest concentration of radioactive label (20%) was detected in thyroid gland, and only 5% in liver. In case of Feridex about 60% of injected dose was captured by liver at 24h, detected using ^{59}Fe-nanoparticles.[24] We believe that MNP-BSA_{Cl} shell was degraded by intracellular proteases after capture of nanoparticles by reticuloendothelial system, and this led to release of free ^{125}I labeled tyrosine residues into blood. Thus, free I^{125}-tyrosine residues accumulated in thyroid gland and quickly removed from organism, probably leaving some MNPs, which we could not effectively monitor.

ACCEPTED MANUSCRIPT

PEGylation of nanoparticles is one of the most common ways to decrease their unspecific uptake by reticuloendothelial system and increase the plasma circulation time.[26] For example, PEGylation of MNPs resulted in an increase of their plasma half-life approximately 5 times compared to non-PEGylated MNPs of the same size.[11] In our case NH_2-PEG-MAL linker was used as a PEGylation agent as well as a linker for attachment of the targeting groups to the nanoparticle surface. A major concern when mAb are conjugated to the nanoparticles is a loss of the antibody binding affinity. In our case after the conjugation of the mAbVEGF to MNP-BSA_{Cl} to the antibodies retained the ability to bind to recombinant VEGF and promoted accumulation of MNP-BSA_{Cl}-mAbVEGF in the VEGF-positive glioma C6 cells.

To evaluate the influence of mAbVEGF on the MRI visualization of brain tumors we used rats with intracranial C6 glioma. The MRI data for MNP-BSA_{Cl}-mAbVEGF and MNP-BSA_{Cl}-IgG injected animals revealed that both contrast agents were able to visualize microvessels of glioma at the early time points (up to 2h) and could act as agents for magnetic resonance angiography. However, 24h after administration only the VEGF-targeted MNP-BSA_{Cl} nanoparticles appeared to be retained in glioma, presumably due to specific binding of these nanoparicles with VEGF over-expressing cells.[23,27] Thus, the specific targeted MNP increased the signal intensity of tumor vasculature immediately after *i.v.* injection as well as detected the areas with most active neoangiogenesis 24h after administration. Altogether we demonstrated that the MNP-BSA_{Cl}-mAbVEGF was more effective tumor MRI visualization agent than the same doses of Feridex or nonspecific MNP-BSA_{Cl}-IgG using an intracranial glioma C6 model in rats.

Here we reported synthesis and characterization of targeted iron oxide nanoparticles suitable as T2 contrast agent for MRI. Coating of the nanoparticles by BSA followed by BSA cross-linking increased the stability of the nanoparticles in aqueous dispersions. The BSA layer also enabled conjugation of mAb to the nanoparticle surface due to presence of many functional groups on the surface. The VEGF targeted MNPs efficiently bound to the VEGF-positive glioma

ACCEPTED MANUSCRIPT

C6 cells compared to nonspecific IgG-modified MNPs. MRI analysis of rats with intracranial glioma C6 revealed that both nanoparticles can be used for tumor and tumor vessels visualization at the early time points after administration. However only VEGF-targeted nanoparticles were able to selectively detect the glioma tumor areas 24h post-injection.

ACCEPTED MANUSCRIPT

ACCEPTED MANUSCRIPT

TABLES

Table 1. Physicochemical characteristics of MNP-BSA, MNP-BSA_{Cl}, MNP-BSA_{Cl}-mAbVEGF and MNP-BSA_{Cl}-IgG in PBS.

FIGURES

Figure 1. Representative TEM image (A) and ring electron diffraction pattern (B) of iron oxide MNPs. The rings are indexed on a face-centered cubic lattice of magnetite Fe_3O_4.

Figure 2. Images of BSA-coated (A) and cross-linked BSA-coated nanoparticles MNPs (B). Top two panels: HAADF-STEM images of MNP-BSA nanoparticles at different magnifications. Note high crystallinity of the particles embedded into amorphous shell. Two middle panels: HAADF-STEM image of the nanoparticles and the corresponding mixed EDX compositional map. Three bottom panels: elemental EDX maps for C, O and Fe.

Figure 3. Diameter (A) and PDI (B) of MNP-BSA and MNP-BSA_{Cl} in PBS containing 10% FBS at 37°C.

Figure 4. PK study of the ^{125}I labeled MNP-BSA_{Cl} (A,B) and cytotoxicity of MNP-BSA_{Cl} in glioma C6 cells, HEK293 and normal rat astrocytes (C), 24 h incubation. The panels present (A) serum PK and (B) organ biodistribution at 24 hr after *i.v.* injection.

Figure 5. Immunofluorescene analysis of MNP-BSA_{Cl}-mAbVEGF (A) and MNP-BSA_{Cl}-IgG (B) on fixed culture of glioma C6 cells. Concentration of Fe 2 μg/mL, magnification ×1000, oil immersion. ELISA analysis of specific and non-specific targeted nanoparticles, MNP-BSA_{Cl}-mAbVEGF and MNP-BSA_{Cl}-IgG (C).

Figure 6. SWI MR images of rats bearing experimental glioma C6 before injection of contrast agents (A, D, G). MR images of gliomas using contrast agents MNP-BSA_{Cl}-IgG (left column), MNP-BSA_{Cl}-mAbVEGF (middle column), Feridex (right column): 5 min (B, E, H) and 24 hours (C, F, I) after *i.v.* injection.

ACCEPTED MANUSCRIPT

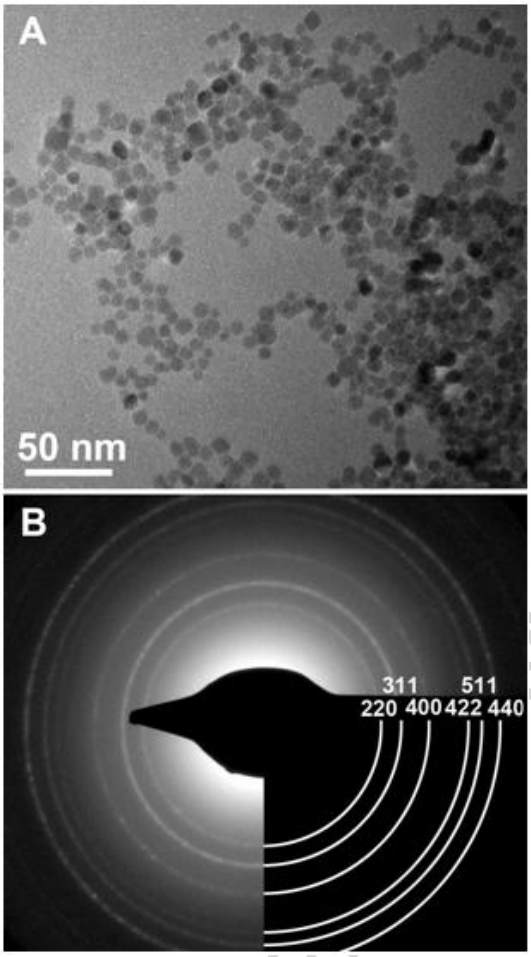

Figure 1

ACCEPTED MANUSCRIPT

ACCEPTED MANUSCRIPT

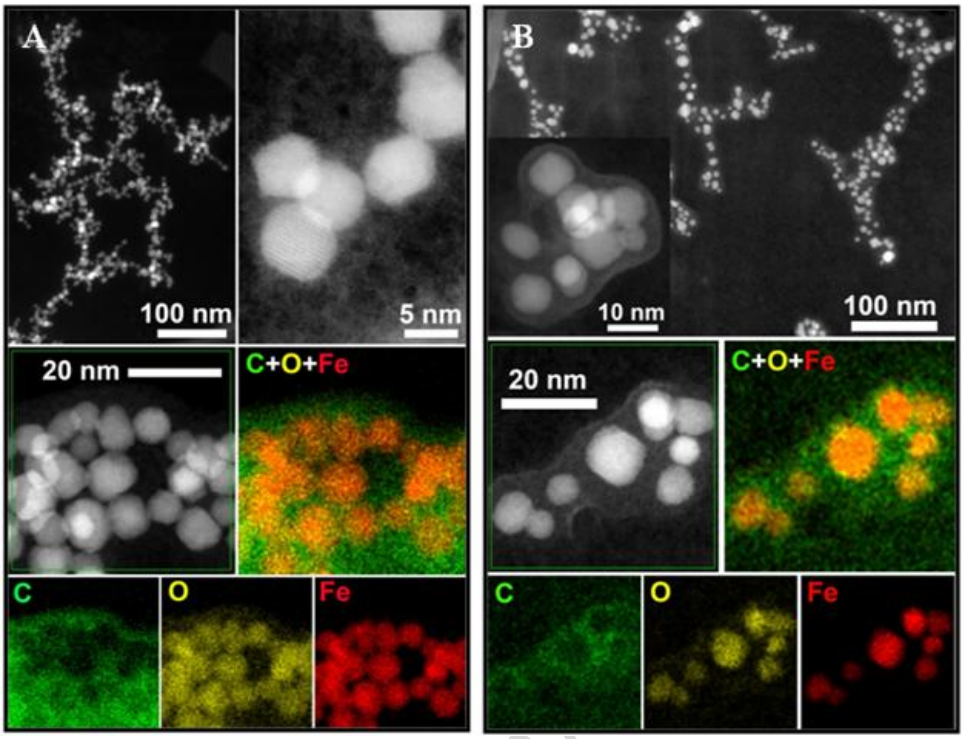

Figure 2

ACCEPTED MANUSCRIPT

ACCEPTED MANUSCRIPT

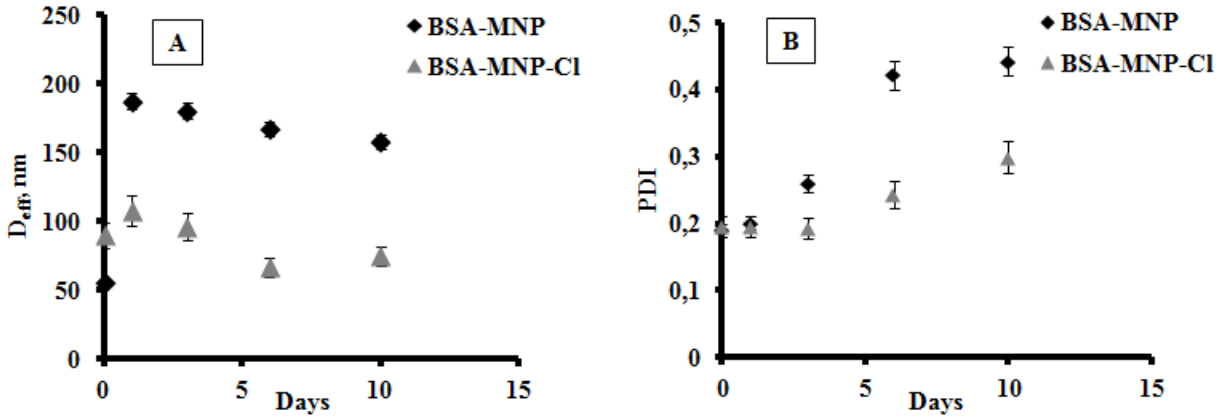

Figure 3

ACCEPTED MANUSCRIPT

ACCEPTED MANUSCRIPT

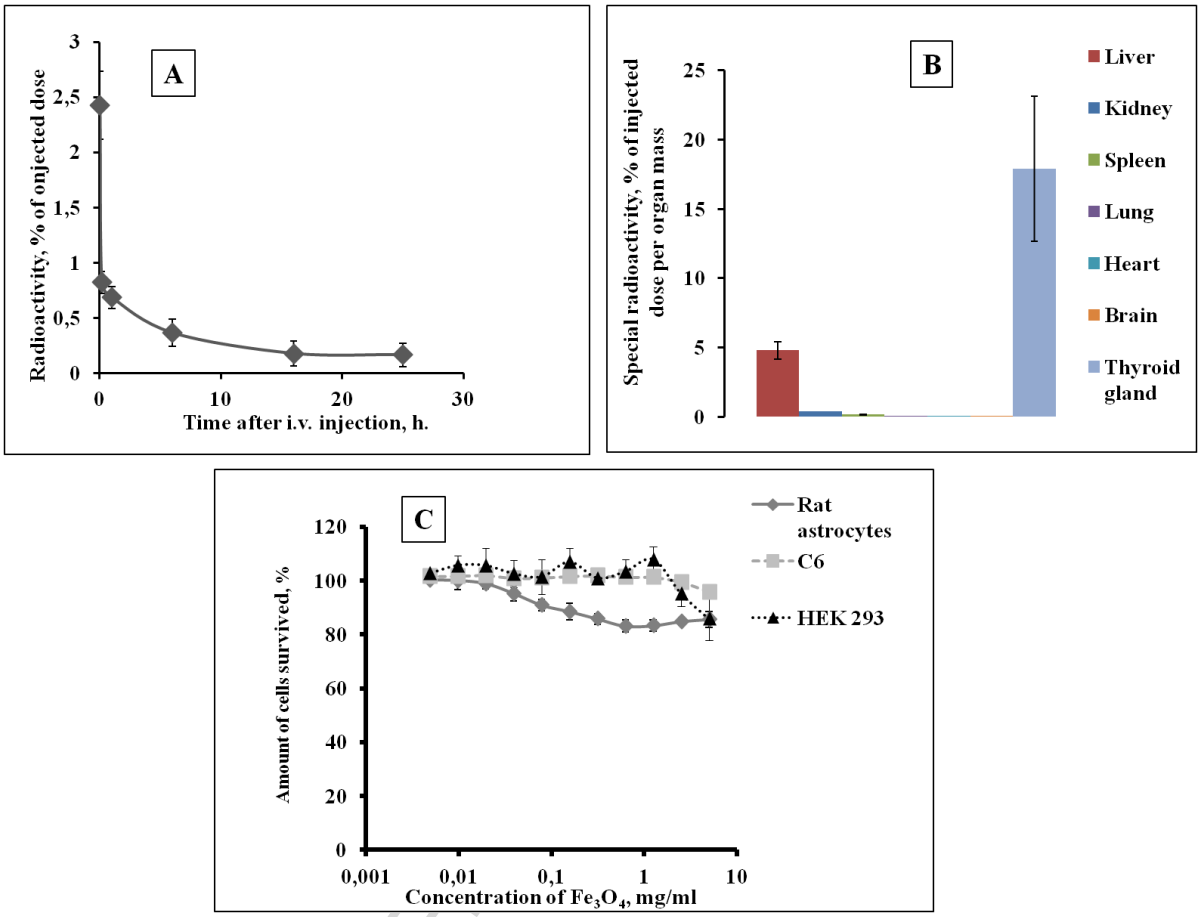

Figure 4

ACCEPTED

ACCEPTED MANUSCRIPT

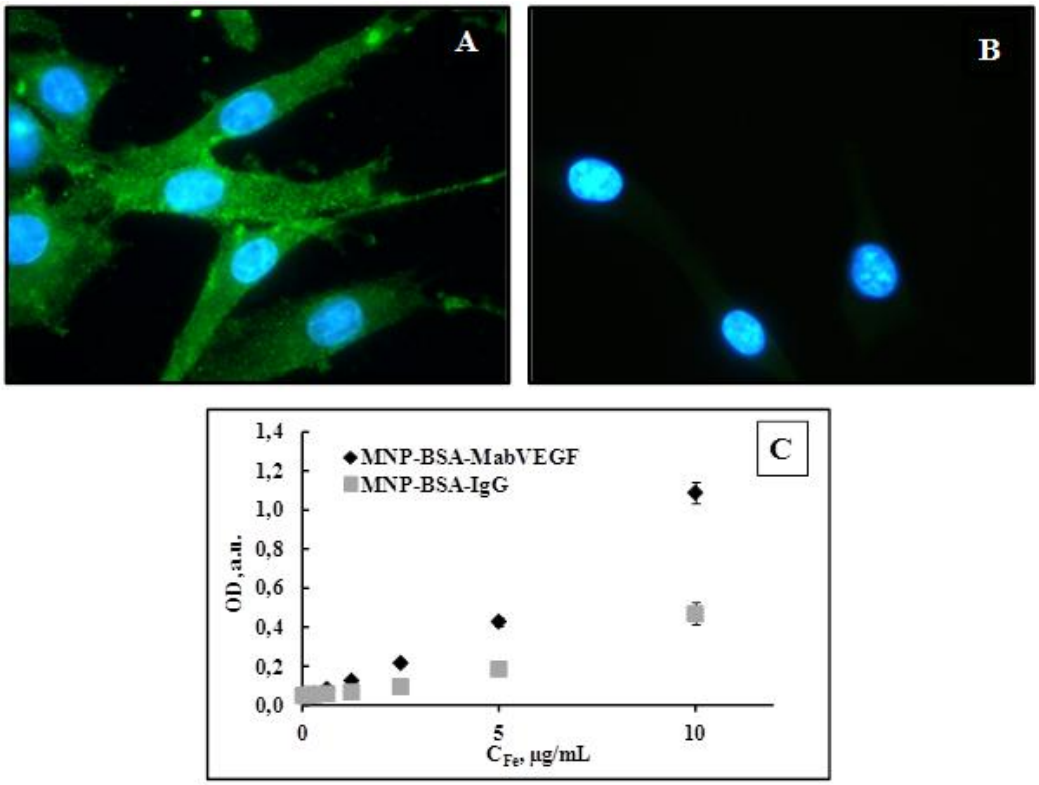

Figure 5

ACCEPTED

ACCEPTED MANUSCRIPT

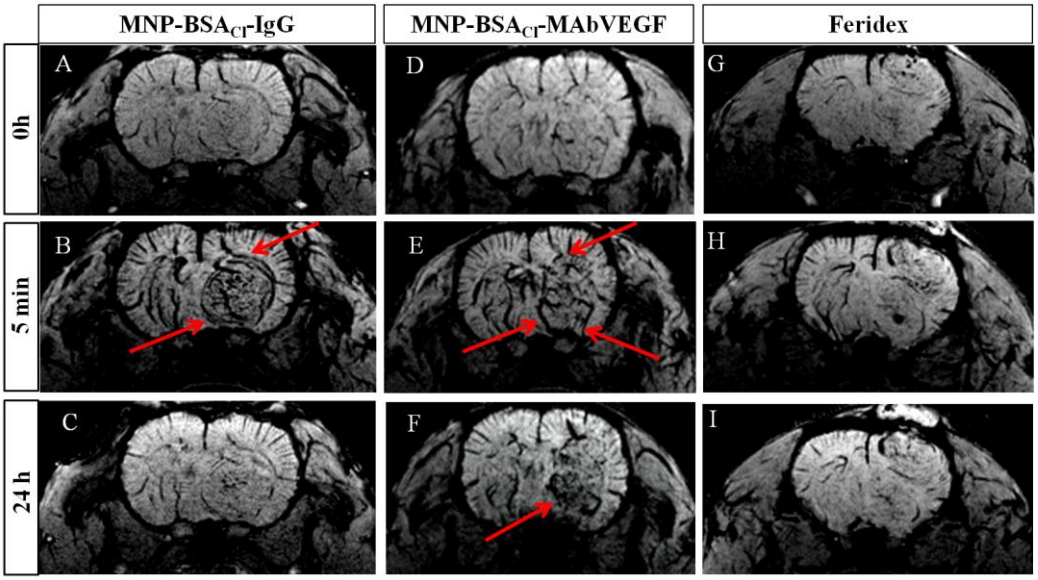

Figure 6

ACCEPTED MANUSCRIPT

ACCEPTED MANUSCRIPT

	MNP-BSA	MNP-BSA_{Cl}	MNP-BSA_{Cl}-mAbVEGF	MNP-BSA_{Cl}-IgG
D_{eff}, nm	53±9	90±2	96±5	101±4
ζ-potential, mV	-41±6	-35±4	-31±5	-32±3
PDI	0.190±0.015	0.196±0.013	0.197±0.012	0.164±0.021
T2 relaxivity, $mM^{-1}s^{-1}$	260±40	216±7	172±2	174±10

Table 1

ACCEPTED MANUSCRIPT

ACCEPTED MANUSCRIPT

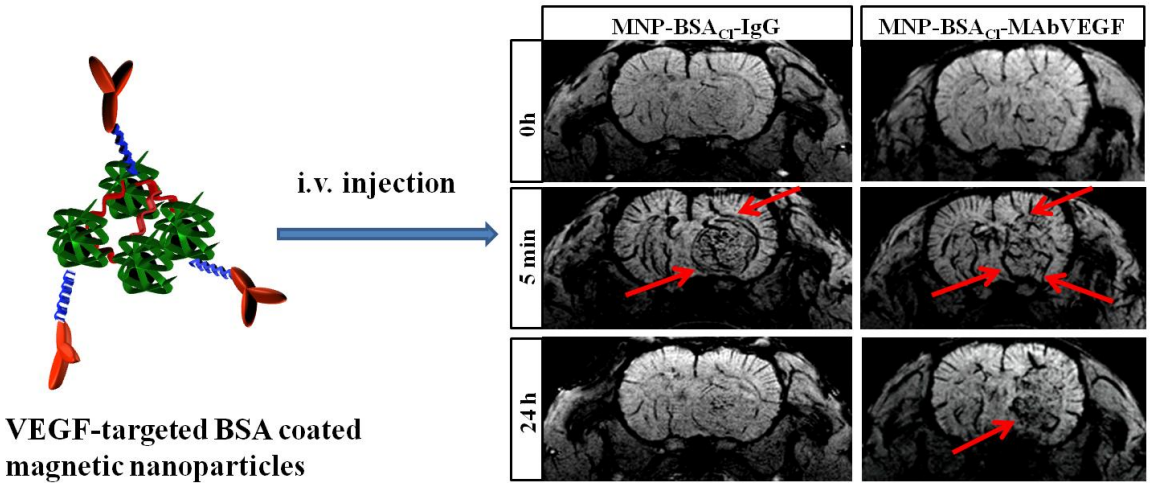

Graphical abstract

MRI is one of the most powerful tools for tumor diagnostics, but still it has some limitations, which mostly associated with poor contrast between normal and pathological tissues. One approach to improve contrast in MRI is the use of contrast agent, such as magnetic iron oxide nanoparticles. In this study, we present VEGF-targeted iron oxide nanoparticles that act as glioma targeted T2 contrast agent, which can visualize brain tumor by MRI 24 h post intravenous injection.

ACCEPTED MANU

ACCEPTED MANUSCRIPT

REFERENCES

(1) Rizvi S, Asghar AH, Mehboob J. Gliosarcoma: A rare variant of glioblastoma multiforme. *J. Pak. Med. Assoc* 2010; **9**:773-775.

(2) Giannopoulos S, Kyritsis AP. Diagnosis and management of multifocal gliomas. *Oncology* 2010;**79**:306-312.

(3) Barnhart JL, Kuhnert N, Bakan DA, Berk RN. Biodistribution of $GdCl_3$ and Gd-DTPA and their influence on proton magnetic relaxation in rat tissues. *Magn. Reson. Imaging* 1987;**5**:221-231.

(4) ABLAVAR® [package insert]. North Billerica, MA: Lantheus Medical Imaging, Inc.;2011.

(5) Pankhurst QA, Connolly J, Jones, SK, Dobson J. Applications of magnetic nanoparticles in biomedicine *J. Phys. D: Appl. Phys.* 2003;**36**:167–181.

(6) Peng X, Qian X, Mao H, Wang AY, Chen ZG, Nie S, et al. Targeted magnetic iron oxide nanoparticles for tumor imaging and therapy. *Int. J. Nanomedicine* 2008;**3**:311-321.

(7) Santana SD, Dhadge VL, Roque AC. Dextran-coated magnetic supports modified with a biomimetic ligand for IgG purification. *ACS Appl. Mater. Interfaces* 2012;**4**:5907-5914.

(8) Laurent S, Forge D, Port M, Roch A, Vander EL, Muller R. Magnetic Iron Oxide Nanoparticles: Synthesis, Stabilization, Vectorization, Physicochemical Characterizations, and Biological Applications *Chem. Rev.* 2008;**108**:2064–2110

(9) Yu M, Huang S, Yu KJ, Clyne AM. Dextran and Polymer Polyethylene Glycol (PEG) Coating Reduce Both 5 and 30 nm Iron Oxide Nanoparticle Cytotoxicity in 2D and 3D Cell Culture. *Int. J. Mol. Sci.* 2012;**13**:5554-5570.

(10) Ferguson RM, Minard KR, Krishnan KM. Optimization of nanoparticle core size for magnetic particle imaging. *J. Magn. Magn. Mater*. 2009;**321**:1548–1551.

(11) Roohi F, Lohrke J, Ide A, Schütz G, Dassler K. Studying the effect of particle size and coating type on the blood kinetics of superparamagnetic iron oxide nanoparticles. *Int. J. Nanomedicine* 2012;**7**:4447-4458.

(12) Wiogo HT, Lim M, Bulmus V, Yun J, Amal R. Stabilization of magnetic iron oxide nanoparticles in biological media by fetal bovine serum (FBS). Langmuir 2011;**27**;843–850.

(13) Yang Q, Liang J, Han H. Probing the interaction of magnetic iron oxide nanoparticles with bovine serum albumin by spectroscopic techniques. *J. Phys. Chem. B.* 2009;**113**:10454–10458.

(14) Norden AD, Drappatz J, Wen PY. Antiangiogenic therapies for high-grade glioma. *Nat. Rev. Neurol*. 2009;**5**: 610–620.

ACCEPTED MANUSCRIPT

(15) Ancopoulos GD, Davis S, Gale NW, Wiegand, SJ, Holash J. Vascular-specific growth factors and blood vessel formation. *Nature* 2000;**407**;242–*248.*

(16) Plate KH, Breier G, Weich HA, Risau W. Vascular endothelial growth factor is a potential tumour angiogenesis factor in human gliomas in vivo. *Nature* 1992;**359**;845 -848.

(17) Schneider SW, Ludwig T, Tatenhorst L, Braune S, Oberleithner H, Senner V, et al. *Acta Neuropathologica* 2004;**107**;272-276.

(18) Shein SA, Gurina OI, Leopol'd AV, Baklaushev VP, Korchagina AA, Grinenko NF, et al. Generation of monoclonal antibodies to recombinant vascular endothelial growth factor. *Bull Exp Biol Med.* 2012;**153**;139-142.

(19) Hunter WM, Greenwood FC. Preparation of iodine-131 labelled human growth hormone of high specific activity. *Nature* 1962;**194**:495-496.

(20) Paul CA, Beltz B, Berger-Sweeney J. Perfusion of Brain Tissues with Fixative. *Cold Spring Harbor Protocols*, 2008;**3**:1-4.

(21) Chekhonin VP, Baklaushev VP, Yusubalieva GM, Pavlov KA, Ukhova OV, Gurina OI. Modeling and immunohistochemical analysis of C6 glioma in vivo. *Bull Exp Biol Med*. 2007;**143**:501-509.

(22) Chen K, Xie J, Xu H, Behera D, Michalski MH, Biswal S, et al. Triblock copolymer coated iron oxide nanoparticle conjugate for tumor integrin targeting. *Biomaterials* 2009;**30**:6912-6919.

(23) Ferrara N. Vascular Endothelial Growth Factor as a target for anticancer therapy. *The Oncologist* 2004;**9**;2-10.

(24) Majumdar S, Zoghbi SS, Gore JC. Pharmacokinetics of superparamagnetic iron-oxide MR contrast agents in the rat. *Invest Radiol.* 1990;**25**:771-777.

(25) Kratz F. Albumin as a drug carrier: Design of prodrugs, drug conjugates and nanoparticles. *J. Control. Release* 2008;**132**;171–183.

(26) Amoozgar Z, Yeo Y. Recent advances in stealth coating of nanoparticle drug delivery systems. *Wiley Interdiscip. Rev. Nanomed. Nanobiotechnol.* 2012;**4**:219-233.

(27) Schmidt NO, Westphal M, Hagel C, Ergün S, Stavrou D, Rosen EM, et al. evels of vascular endothelial growth factor, hepatocyte growth factor/scatter factor and basic fibroblast growth factor in human gliomas and their relation to angiogenesis. *Int. J. Cancer* 1999;**84**:10-18.